IEEE Access
Multidisciplinary | Rapid Review | Open Access Journal

Received September 26, 2020, accepted November 3, 2020, date of publication November 9, 2020,
date of current version November 20, 2020.

Digital Object Identifier 10.1109/ACCESS.2020.3036613

Magnetic Field Calculation of a Novel Electromagnetic Clutch Based on an Interpolating Element-Free Galerkin Method

FAN YANG AND CHENGLIN GU

State Key Laboratory of Advanced Electromagnetic Engineering and Technology, School of Electrical and Electronic Engineering, Huazhong University of Science and Technology, Wuhan 430074, China

Corresponding author: Fan Yang (yangfanchn@hust.edu.cn)

This work was supported by the National Natural Science Foundation of China under Grant 51377063.

ABSTRACT In this paper, the interpolating element-free Galerkin method (IEFGM) is introduced to calculate the magnetic field distribution of a novel permanent magnet bistable electromagnetic clutch (BPMEC), which is used in the in-wheel motor drive system to flexibly connecting the wheel and motor to release the mechanical shock and electromagnetic impulsion. Firstly, the fundamental of the IEFGM is introduced, and a new weight function for magnetic field calculation is proposed. Then the nodes distribution is discussed, and the magnetic field distribution of the clutch is analyzed. Simulation results show the IEFGM can impose the boundary conditions directly and fewer nodes are employed, make the calculation efficiency higher. Finally, some experiments are carried out, the experimental results verified the effectiveness of the IEFGM in magnetic field calculation. The study results provide references for the application of the interpolating element-free Galerkin method in the magnetic field calculation.

INDEX TERMS Meshless method, interpolating element-free Galerkin method (IEFGM), magnetic field calculation, electromagnetic clutch.

I. INTRODUCTION

Because of its simple mathematical structure and great versatility, the finite element method (FEM) is the most widely used solution method for potential problems [1]. However, the FEM is difficult in some complicated problems, such as fracture analysis and moving conductor problems. The domain of these problems needs remesh at every step during the simulation, resulting in loss of accuracy. Thus meshless methods that do not require a mesh are developed, and the most practical of them is the element-free Galerkin method (EFGM) which was first proposed and developed by Belytschko *et al.* in [2]–[5]. In the field of electromagnetic field calculation, the EFGM has also been applied and improved [6]–[10].

The discrete equations of the EFGM and the FEM are the same, and the only difference between the FEM and the EFGM is the construction methods of the shape function. Compared with the FEM, the EFGM use moving least-squares (MLS) approximation to obtain the shape function and it only requires a set of nodes and a description of boundary conditions. However, the shape function obtained by MLS approximation does not satisfy the property of Kronecker delta function, so the essential boundary conditions cannot be imposed directly [11], [12]. Therefore, some additional methods are required to apply the boundary conditions, such as penalty methods and Lagrange multiplier methods.

Authors of [13] presented an interpolating moving least-squares (IMLS) method which can obtain the shape function that satisfied the property of Kronecker delta function, thus the boundary conditions can be applied directly as in FEM, and the error estimates of this method are discussed in [14]. Based on the IMLS method, the interpolating element-free Galerkin method (IEFGM) with higher computational efficiency is derived [13]. The IEFGM has been discussed in two-dimensional and three-dimensional potential problems [13], [15], and also be used to solve elastoplasticity problems [16], [17]. However, the application of the IEFGM in specific magnetic field calculations has not yet been studied.

In this paper, the interpolating element-free Galerkin method is introduced to calculate the magnetic field

The associate editor coordinating the review of this manuscript and approving it for publication was Su Yan.

distribution of a novel permanent magnet bistable electromagnetic clutch (BPMEC). The clutch is used in the in-wheel motor drive system to flexibly connecting the wheel and motor. The mechanical shock and electromagnetic impulsion in the drive system can be significantly reduced through this flexible connection [18]–[21]. As the clutch works in a self-holding steady state most of the time, the holding force in steady state is the most important index, thus the magnetic field analysis needs to be discussed.

This paper developed the magnetic field analysis of the clutch based on the IEFGM, and the comparison with the FEM and experimental results verified the effectiveness of the IEFGM in magnetic field calculations. First, the fundamental of the MLS and the IMLS method is introduced. Second, the structure of the electromagnetic clutch is described and the boundary conditions, as well as discrete equations, are presented. Then a new weight function is proposed and the magnetic field distribution is discussed. Finally, experiments are carried out to validate the effectiveness of the IEFGM. The study results provide references for the application of the IEFGM in magnetic field calculation.

II. MLS METHOD

Assume the field function is $u(\boldsymbol{x})$, where $\boldsymbol{x} = (x, y)$ in two-dimensional, and the value of n nodes are given by (1):

$$u(\boldsymbol{x}_i) = u_i, \quad (i = 1, 2, \cdots, n) \tag{1}$$

the vector form is:

$$\boldsymbol{u} = [u_1, u_2, \cdots, u_n]^{\mathrm{T}} \tag{2}$$

Define the trial function as:

$$u^h(\boldsymbol{x}) = \boldsymbol{p}^{\mathrm{T}}(\boldsymbol{x})\boldsymbol{a}(\boldsymbol{x}) \tag{3}$$

where $\boldsymbol{p}(\boldsymbol{x})$ is the basis function, $\boldsymbol{a}(\boldsymbol{x})$ is the coefficients. In 2D, the basis function is defined as follows.

$$\text{Linear basis: } \boldsymbol{p}^{\mathrm{T}}(\boldsymbol{x}) = [1, x, y] \tag{4}$$

$$\text{Quadratic basis: } \boldsymbol{p}^{\mathrm{T}}(\boldsymbol{x}) = [1, x, y, x^2, xy, y^2] \tag{5}$$

In order to determine the coefficients $\boldsymbol{a}(\boldsymbol{x})$, a weighted function is introduced as:

$$J = \sum_{i=1}^{n} w(\boldsymbol{x} - \boldsymbol{x}_i)[\boldsymbol{p}^{\mathrm{T}}(\boldsymbol{x}_i)\boldsymbol{a}(\boldsymbol{x}) - u_i]^2 \tag{6}$$

where $w(\boldsymbol{x} - \boldsymbol{x}_i)$ is the weight function with compact support property, the coefficients can be obtained by minimizing J, as in (7).

$$\boldsymbol{a}(\boldsymbol{x}) = \boldsymbol{A}^{-1}(\boldsymbol{x})\boldsymbol{B}(\boldsymbol{x})\boldsymbol{u} \tag{7}$$

where

$$\boldsymbol{A}(\boldsymbol{x}) = \sum_{i=1}^{n} w(\boldsymbol{x} - \boldsymbol{x}_i)\boldsymbol{p}(\boldsymbol{x}_i)\boldsymbol{p}^{\mathrm{T}}(\boldsymbol{x}_i) \tag{8}$$

and

$$\boldsymbol{B}(\boldsymbol{x}) = [w(\boldsymbol{x} - \boldsymbol{x}_1)\boldsymbol{p}(\boldsymbol{x}_1), \cdots, w(\boldsymbol{x} - \boldsymbol{x}_n)\boldsymbol{p}(\boldsymbol{x}_n)] \tag{9}$$

Substituting (7) into (3), the trail function is derived as:

$$u^h(\boldsymbol{x}) = \sum_{i=1}^{n} N_i(\boldsymbol{x})u_i \tag{10}$$

where $N_i(\boldsymbol{x})$ is the shape function and

$$\boldsymbol{N}(\boldsymbol{x}) = [N_1(\boldsymbol{x}), \cdots, N_n(\boldsymbol{x})] = \boldsymbol{p}^T(\boldsymbol{x})\boldsymbol{A}^{-1}(\boldsymbol{x})\boldsymbol{B}(\boldsymbol{x}) \tag{11}$$

In the MLS, the shape function does not satisfy the property of Kronecker delta function as:

$$N_i(\boldsymbol{x}_j) = \begin{cases} 1, & i = j \\ 0, & i \neq j \end{cases} \tag{12}$$

so the boundary conditions cannot be applied directly.

III. IMLS METHOD

Compared with the MLS, the IMLS method revised the basis function $\boldsymbol{p}(\boldsymbol{x})$. $p_1(\boldsymbol{x})$ is normalized as:

$$b_{\boldsymbol{x}}^{(1)} = \frac{1}{\left[\sum_{i=1}^{n} w(\boldsymbol{x} - \boldsymbol{x}_i)\right]^{1/2}} \tag{13}$$

for $j = 2, 3, \ldots,$ m, the functions are generated as follows:

$$b_{\boldsymbol{x}}^{(j)}(\mathbf{x}) = p_j(\mathbf{x}) - \sum_{i=1}^{n} p_j(\boldsymbol{x}_i)v(\boldsymbol{x} - \boldsymbol{x}_i) \tag{14}$$

where

$$v(\boldsymbol{x} - \boldsymbol{x}_i) = \frac{w(\boldsymbol{x} - \boldsymbol{x}_i)}{\sum_{i=1}^{n} w(\boldsymbol{x} - \boldsymbol{x}_i)} \tag{15}$$

Using the new basis functions $b_{\boldsymbol{x}}^{(1)}(\mathbf{x}), \ldots, b_{\boldsymbol{x}}^{(m)}(\mathbf{x})$, the corresponding trail function is:

$$u^h(\boldsymbol{x}) = \boldsymbol{v}^{\mathrm{T}}(\boldsymbol{x})\boldsymbol{u} + \boldsymbol{b}^{\mathrm{T}}(\boldsymbol{x})\boldsymbol{a}(\boldsymbol{x}) \tag{16}$$

where

$$\boldsymbol{v}(\boldsymbol{x}) = [\boldsymbol{v}(\boldsymbol{x} - \boldsymbol{x}_1), \boldsymbol{v}(\boldsymbol{x} - \boldsymbol{x}_2), \cdots, \boldsymbol{v}(\boldsymbol{x} - \boldsymbol{x}_n)]^{\mathrm{T}} \tag{17}$$

$$b(\boldsymbol{x}) = [b_{\boldsymbol{x}}^{(2)}(\boldsymbol{x}), b_{\boldsymbol{x}}^{(3)}(\boldsymbol{x}), \cdots, b_{\boldsymbol{x}}^{(m)}(\boldsymbol{x})]^{\mathrm{T}} \tag{18}$$

Then according to the MLS approximation, the coefficients are expressed by (19),

$$\boldsymbol{a}(\boldsymbol{x}) = \boldsymbol{A}_{\boldsymbol{x}}^{-1}(\boldsymbol{x})\boldsymbol{B}_{\boldsymbol{x}}(\boldsymbol{x})\boldsymbol{u} \tag{19}$$

where

$$\boldsymbol{A}_{\boldsymbol{x}}(\boldsymbol{x}) = \sum_{i=1}^{n} w(\boldsymbol{x} - \boldsymbol{x}_i)\boldsymbol{b}(\boldsymbol{x}_i)\boldsymbol{b}^{\mathrm{T}}(\boldsymbol{x}_i) \tag{20}$$

and

$$\boldsymbol{B}_{\boldsymbol{x}}(\boldsymbol{x}) = [w(\boldsymbol{x} - \boldsymbol{x}_1)\boldsymbol{b}(\boldsymbol{x}_1), \cdots, w(\boldsymbol{x} - \boldsymbol{x}_n)\boldsymbol{b}(\boldsymbol{x}_n)] \tag{21}$$

Equation (16) can be written as:

$$u^h(\boldsymbol{x}) = \boldsymbol{N}(\boldsymbol{x})\boldsymbol{u} \tag{22}$$

where the new shape function is:

$$\boldsymbol{N}(\boldsymbol{x}) = \boldsymbol{v}^{\mathrm{T}}(\boldsymbol{x}) + \boldsymbol{b}^{\mathrm{T}}(\boldsymbol{x})\boldsymbol{A}_{\boldsymbol{x}}^{-1}(\boldsymbol{x})\boldsymbol{B}_{\boldsymbol{x}}(\boldsymbol{x}) \tag{23}$$

and the partial derivative of the shape function is:

$$\begin{aligned}\boldsymbol{N}(\boldsymbol{x})_{,k} = {} & \boldsymbol{v}^{\mathrm{T}}(\boldsymbol{x})_{,k} + \boldsymbol{b}^{\mathrm{T}}(\boldsymbol{x})_{,k}\boldsymbol{A}_{\boldsymbol{x}}^{-1}(\boldsymbol{x})\boldsymbol{B}_{\boldsymbol{x}}(\boldsymbol{x}) \\ & + \boldsymbol{b}^{\mathrm{T}}(\boldsymbol{x})\boldsymbol{A}_{\boldsymbol{x}}^{-1}(\boldsymbol{x})_{,k}\boldsymbol{B}_{\boldsymbol{x}}(\boldsymbol{x}) + \boldsymbol{b}^{\mathrm{T}}(\boldsymbol{x})\boldsymbol{A}_{\boldsymbol{x}}^{-1}(\boldsymbol{x})\boldsymbol{B}_{\boldsymbol{x}}(\boldsymbol{x})_{,k}\end{aligned} \tag{24}$$

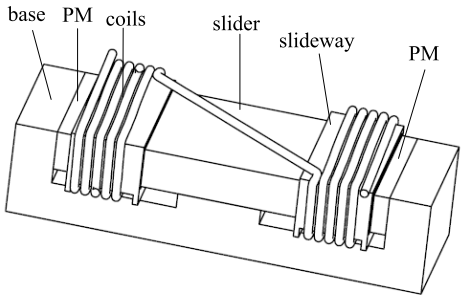

FIGURE 1. The structure of BPMEC.

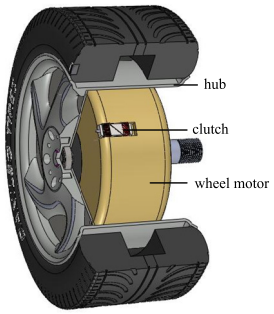

FIGURE 2. The assembly diagram.

where k is x or y, and

$$\boldsymbol{A}_{\boldsymbol{x}}^{-1}(\boldsymbol{x})_{,k} = -\boldsymbol{A}_{\boldsymbol{x}}^{-1}(\boldsymbol{x})\boldsymbol{A}_{\boldsymbol{x}}(\boldsymbol{x})_{,k}\boldsymbol{A}_{\boldsymbol{x}}^{-1}(\boldsymbol{x}) \tag{25}$$

$$\boldsymbol{v}(\boldsymbol{x}-\boldsymbol{x}_i)_{,k} = \frac{w(\boldsymbol{x}-\boldsymbol{x}_i)_{,k}}{\sum_{i=1}^{n} w(\boldsymbol{x}-\boldsymbol{x}_i)} - \frac{-w(\boldsymbol{x}-\boldsymbol{x}_i)\sum_{i=1}^{n} w(\boldsymbol{x}-\boldsymbol{x}_i)_{,k}}{(\sum_{i=1}^{n} w(\boldsymbol{x}-\boldsymbol{x}_i))^2} \tag{26}$$

$$\boldsymbol{b}^{(j)}(\boldsymbol{x})_{,k} = p_j(x)_{,k} - \sum_{i=1}^{n} p_j(\boldsymbol{x}_i)\boldsymbol{v}(\boldsymbol{x}-\boldsymbol{x}_i)_{,k} \tag{27}$$

$$\boldsymbol{b}^{(j)}(\boldsymbol{x}_i)_{,k} = -\sum_{i=1}^{n} p_j(\boldsymbol{x}_i)\boldsymbol{v}(\boldsymbol{x}-\boldsymbol{x}_i)_{,k} \tag{28}$$

The new trail function satisfied:

$$u^h(\boldsymbol{x}_i) = u(\boldsymbol{x}_i) \tag{29}$$

thus by the IMLS method, the boundary conditions can be applied as convenient as in the FEM.

IV. THE NOVEL ELECTROMAGNETIC CLUTCH

As shown in Fig. 1, the main components of BPMEC are base, permanent magnet (PM), coils, slider, and slideway. The clutch relies on the magnetic force of the slider imposed by PM to maintain in steady state without energy consumption. When the clutch needs actuation, applied current to coils appropriately, the magnetic force imposed on the slider will change direction and make the slider move to the other side, then turn off the current, the clutch returns to the steady state. The clutch has a compact structure to match the limited available space in the hubs, as illustrated in Fig. 2.

By installing this clutch, the wheel and motor can realize a flexible connection, thus the mechanical shock and electromagnetic impulsion can be released at the starting and braking process of the electric vehicles.

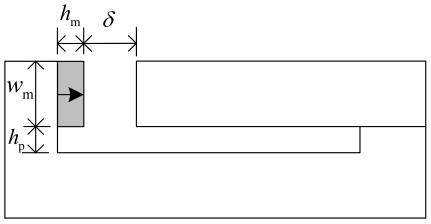

FIGURE 3. The 2D analysis model.

TABLE 1. The main parameters of BPMEC.

Parameters	Values
Thickness of the PM h_m	1.5 mm
Width of the PM w_m	4 mm
Travel length l_x	3 mm
Height h_p	1.5 mm
Remanence of the PM B_r	0.38 T
Coercivity of the PM H_c	-300 kA/m
Relative permeability of slider and base	2000

It can be seen that the clutch structure is symmetric so that the analysis model can be simplified, as shown in Fig. 3, the main parameters are shown in table 1.

V. IEFGM FOR ELECTROMAGNETIC PROBLEMS

A. DISCRETE EQUATIONS

In the electromagnetic field, The boundary problem of the magnetic vector potential is:

$$\frac{\partial}{\partial x}\left(\nu\frac{\partial A_z(\boldsymbol{x})}{\partial x}\right) + \frac{\partial}{\partial y}\left(\nu\frac{\partial A_z(\boldsymbol{x})}{\partial y}\right) = -J_z, \quad \boldsymbol{x}\in\Omega \tag{30}$$

$$A_z(\boldsymbol{x}) = A_0, \quad \boldsymbol{x}\in\Gamma_1 \tag{31}$$

$$\nu\frac{\partial A_z(\boldsymbol{x})}{\partial n} = q, \quad \boldsymbol{x}\in\Gamma_2 \tag{32}$$

The Galerkin weak form of (30)-(32) is:

$$\int_\Omega \nu\delta(\nabla A_z)^{\mathrm{T}}\cdot(\nabla A_z)\mathrm{d}\Omega - \int_\Omega \delta A_z\cdot J_z\mathrm{d}\Omega - \int_{\Gamma_2}\delta A_z\cdot q\mathrm{d}\Gamma = 0 \tag{33}$$

According to the IMLS method, the magnetic vector potential A_z at position $\boldsymbol{x}$ can be expressed as:

$$A_z(\boldsymbol{x}) = N(\boldsymbol{x})A \tag{34}$$

Substituting (34) into (33), the discrete equations can be derived as:

$$\boldsymbol{K}\boldsymbol{A} = \boldsymbol{F} \tag{35}$$

where

$$\boldsymbol{A} = [A_1, A_2, \cdots, A_n]^{\mathrm{T}} \tag{36}$$

$$K_{ij} = \int_\Omega \boldsymbol{v}\left(\frac{\partial N_i}{\partial x}\frac{\partial N_j}{\partial x} + \frac{\partial N_i}{\partial y}\frac{\partial N_j}{\partial y}\right)\mathrm{d}x\mathrm{d}y \tag{37}$$

$$F_i = \int_\Omega J_z N_i\mathrm{d}x\mathrm{d}y + \int_{\Gamma_2} qN_i\mathrm{d}\Gamma \tag{38}$$

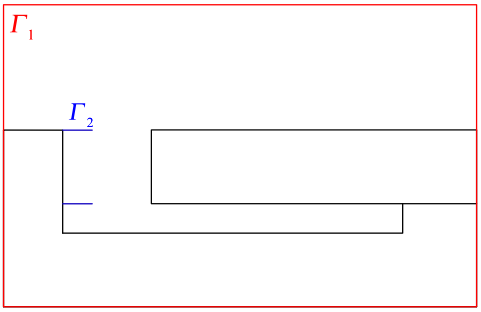

FIGURE 4. The boundary problem model.

Gaussian integration is used to calculate equation (35). Since the value of nodes is obtained, the magnetic flux density in the model can be calculated.

B. THE SELECTION OF WEIGHT FUNCTION

In this paper, a modified weight function for the IEFGM is proposed, as expressed in (39).

$$w(r) = \begin{cases} \dfrac{e^{-(\alpha r)^2}}{r^2}, & r \le 1 \\ 0, & r > 1 \end{cases} \tag{39}$$

where α is an even positive integer, and choose $\alpha = 12$ in this paper.

The rectangular region is selected as the domain of influence, as in (40):

$$w(\boldsymbol{x} - \boldsymbol{x}_i) = w(r_{\boldsymbol{x}})w(r_y) \tag{40}$$

where

$$r_{\boldsymbol{x}} = \frac{|x - x_i|}{d_{mx}} \tag{41}$$

$$r_y = \frac{|y - y_i|}{d_{my}} \tag{42}$$

and

$$d_{mx} = d_m \Delta x \tag{43}$$

$$d_{my} = d_m \Delta y \tag{44}$$

where d_{m} is a scalar parameter that determines the size of the influence domain, and Δx, Δy is the node spacing.

VI. MAGNETIC FIELD CALCULATION OF THE BPMEC

A. BOUNDARY CONDITIONS

As shown in Fig. 4, The magnetic field and boundary conditions of the BPMEC is given by:

$$\frac{\partial}{\partial x}\left(\nu \frac{\partial A_z}{\partial x}\right) + \frac{\partial}{\partial y}\left(\nu \frac{\partial A_z}{\partial y}\right) = 0, \quad \boldsymbol{x} \in \Omega \tag{45}$$

$$A_z = 0, \quad \boldsymbol{x} \in \Gamma_1 \tag{46}$$

$$\nu \frac{\partial A_z}{\partial n} = \pm H_c, \quad \boldsymbol{x} \in \Gamma_2 \tag{47}$$

B. MAGNETIC FIELD DISTRIBUTION

The node distribution on the rectangular model is shown in Fig. 5, 31 × 41 nodes are employed in this calculation, and the weight function (39) as well as the linear basis function (4) are used.

Fig. 6 depicts the magnetic field distribution of the clutch calculated by the interpolating element-free Galerkin method,

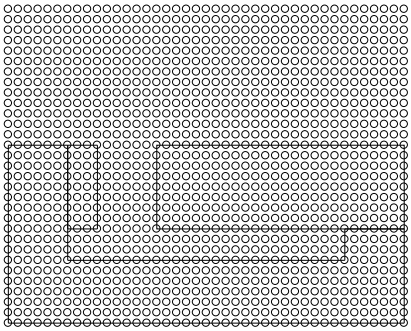

FIGURE 5. The node distribution.

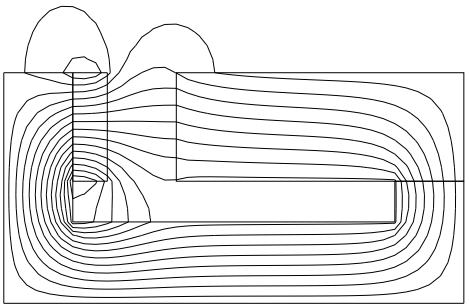

FIGURE 6. The magnetic field distribution by IEFGM (31 × 41 nodes).

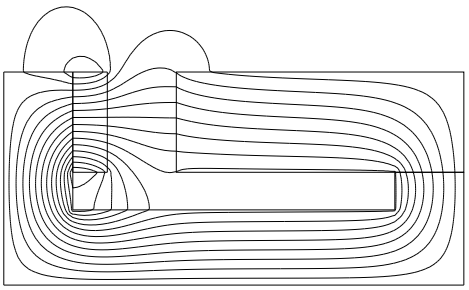

FIGURE 7. The magnetic field distribution by FEM.

which in excellent agreement with the analysis result by FEM shown in Fig. 7. Fig. 8 shows the analysis result where the weight function presented in [13] is used, it can be seen that the magnetic field distribution is deformation. Therefore, the new weight function (39) proposed in this paper is more precise when used in magnetic field calculation by IEFGM. In addition, the calculation result when distributed 61 × 81 nodes is illustrated in Fig. 9. It is observed the magnetic lines of force become smoother, and the magnetic field distribution is the same as the results by FEM.

Further analysis indicated that it is required to distribute 61 × 81 nodes to get a precision result when analyzed by the EFGM, as shown in Fig. 10, and the spent time is 14.8 s. Meanwhile, when calculated by the IEFGM, we can obtain sufficiently accurate results by employ 31 × 41 nodes, and the spent time is 3.2 s. Therefore, the IEFGM has a higher efficiency than EFGM.

C. MAGNETIC FLUX LEAKAGE

The magnetic flux leakage coefficient reflects the holding force of the slider in steady state and the usage of the

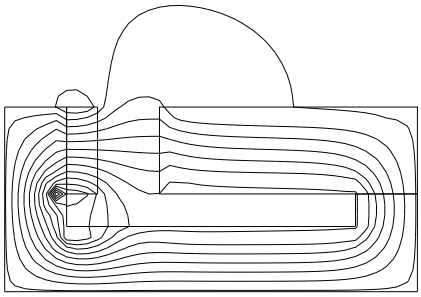

FIGURE 8. The magnetic field distribution by IEFGM (using weight function proposed in [13]).

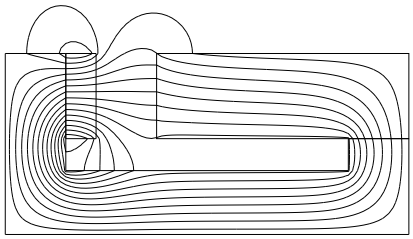

FIGURE 9. The magnetic field distribution by IEFGM (61 × 81 nodes).

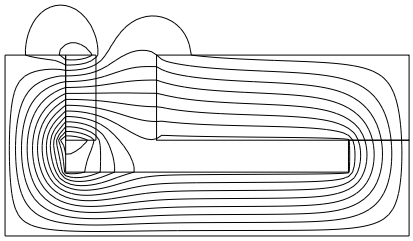

FIGURE 10. The magnetic field distribution by EFGM (61 × 81 nodes).

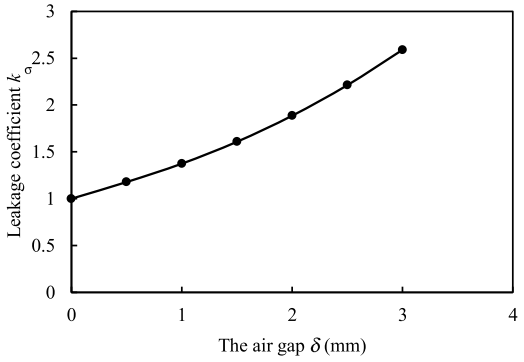

FIGURE 11. The leakage coefficient when the air gap changing.

permanent magnet. Fig. 11 illustrates the curve of the flux leakage coefficient varies with the air gap between the slider and permanent magnet changes. It is clear that with the increase of the air gap, the flux leakage coefficient increases, which means the force imposed on the slider by the permanent magnet decreases.

Table 2 depicts the detailed value of the flux leakage coefficient k_σ calculated by the IEFGM and FEM, it is evident that the result of the IEFGM is very close to FEM. Besides, when the air gap changes, the grids are required to be remeshed when using the FEM; as for the IEFGM, the node distribution

TABLE 2. Detailed value of the flux leakage coefficient.

The air gap δ (mm)	k_σ (by IEFGM)	k_σ (by FEM)
0	1	1
0.5	1.178	1.189
1	1.374	1.383
1.5	1.608	1.616
2	1.886	1.897
2.5	2.212	2.224
3	2.589	2.605

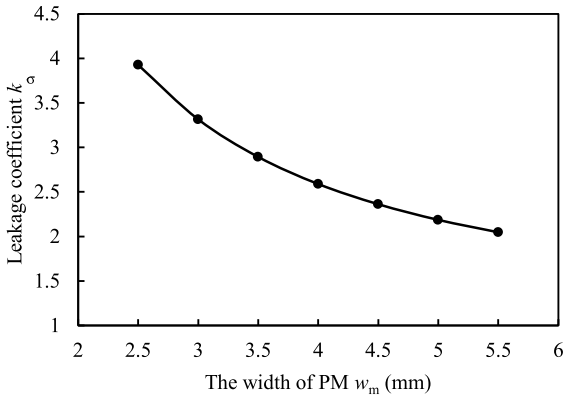

FIGURE 12. The leakage coefficient when the width of PM changing.

shown in Fig. 5 is always employed and no adjustment is required.

Fig. 12 shows the flux leakage coefficient when the width of PM changing, it can be seen that increasing the width of PM can improve the usage of PM, however, the cost of the clutch will be higher, thus the selection of PM width $w_m = 4$ mm.

D. IMPROVEMENT OF THE ANALYSIS MODEL

Compared with the 3D model shown in Fig. 1, it is clear that the 2D analysis model shown in Fig. 2 cannot take the flux leakage on the front and back region of the clutch into account, resulting in the smaller flux leakage. Therefore, the 2D model is improved, and the idea is: firstly, enlarge the magnetic leakage of the upper region by symmetric the upper and lower region; then move the edge of the base to align with the edge of the slider to further compensate the flux leakage. The improved 2D model is shown in Fig. 13, it can compensate the flux leakage on the front and back region, besides, the magnetic field calculation is simpler, and the spent time is 1.5 s which less than half of the spent time by original 2D model.

Fig. 14 illustrates the comparison of the leakage coefficient between the 3D model and improved 2D model, it can be seen that the calculation results of these two methods are quite close when the gap smaller than 1.5 mm, and the maximum relative error is less than 10%.

E. FORCE ANALYSIS

The equivalent magnetic circuit of the clutch is shown in Fig.15. According to Fig. 15, the magnetic circuit equations

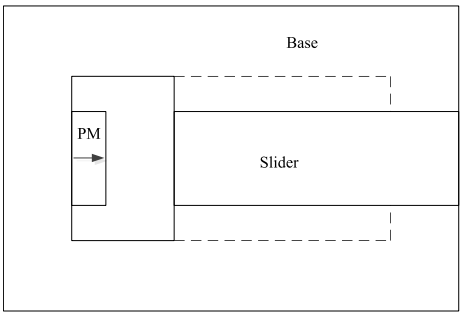

FIGURE 13. The Improved 2D model.

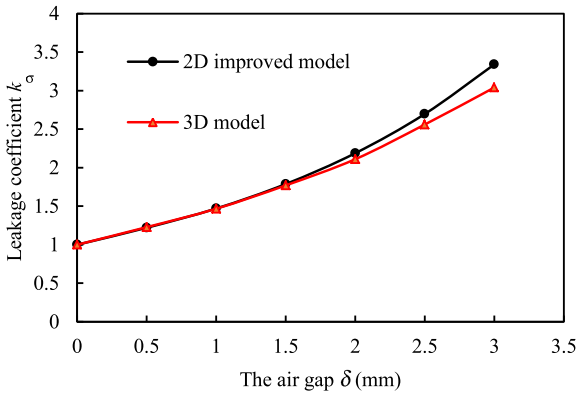

FIGURE 14. The leakage coefficient.

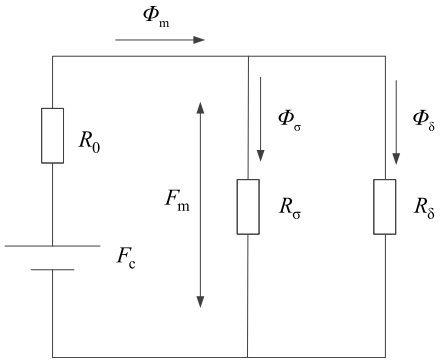

FIGURE 15. The equivalent magnetic circuit.

are express in (48),

$$\begin{cases} F_{\mathrm{m}} = F_{\mathrm{c}} - \Phi_{\mathrm{m}} R_0 \\ F_{\mathrm{m}} = \Phi_\delta R_\delta \\ \Phi_{\mathrm{m}} = k_\sigma \Phi_\delta \end{cases} \tag{48}$$

where

$$F_{\mathrm{c}} = H_{\mathrm{c}} h_{\mathrm{m}} \tag{49}$$

$$R_0 = \frac{h_{\mathrm{m}}}{\mu_0 w_{\mathrm{m}} l_{\mathrm{m}}} \tag{50}$$

$$R_\delta = \frac{\delta}{\mu_0 w_{\mathrm{m}} l_{\mathrm{m}}} \tag{51}$$

The magnetic flux density of the main magnetic circuit is obtained by solve (48), as expressed in (52),

$$B_\delta = \frac{B_{\mathrm{r}}}{k_\sigma + \delta / h_{\mathrm{m}}} \tag{52}$$

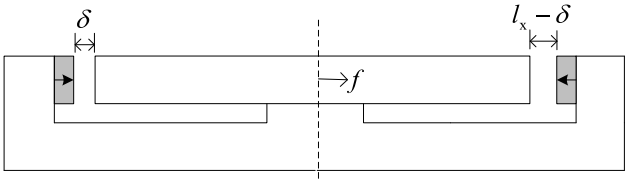

FIGURE 16. The force analysis model.

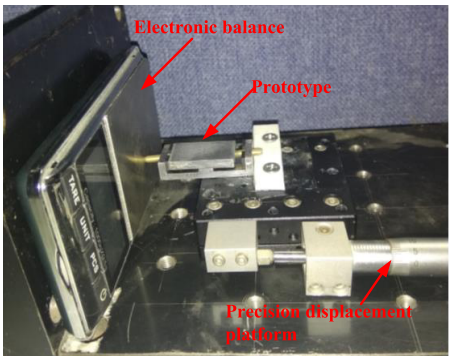

FIGURE 17. The experimental platform.

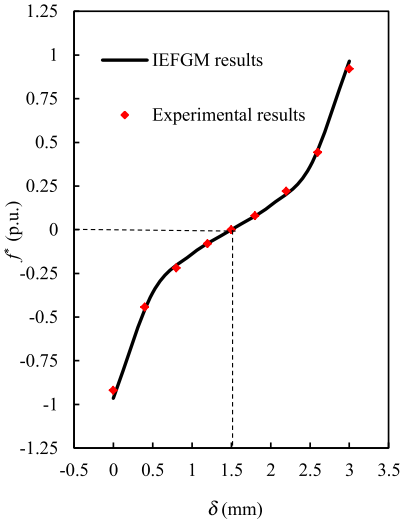

FIGURE 18. The force when slider at different positions.

then based on the virtual displacement method, the force on the slider can be defined by (53).

$$f_\delta = \frac{B_\delta^2}{2\mu_0} w_m l_m \tag{53}$$

The force analysis model is shown in Fig. 16. Define f^* as the per unit value of the force, and the base value is expressed in (54).

$$f_{\mathrm{b}} = \frac{B_{\mathrm{r}}^2}{2\mu_0} w_{\mathrm{m}} l_{\mathrm{m}} \tag{54}$$

VII. EXPERIMENT

In order to validate the magnetic field calculation results by IEFGM, the clutch prototype (without slideway and coils) and experimental platform are built, as shown in Fig. 17.

The holding force of the clutch when the slider at different positions is illustrated in Fig. 18. It is clear that the results

calculated by the IEFGM in excellent agreement with the experimental results. According to Fig. 18, the clutch has two steady states: 'touch' state when the slider close to the permanent magnet on the left side; 'detach' state when the slider is close to the permanent magnet on the right. In addition, when the slider at the center of the clutch, the horizontal force imposed on the slider is zero, but a slight movement of the slider will make the clutch transition to the above steady state, so this is an 'unstable' balanced state. The force on the slider when the clutch in steady state is the holding force, i.e., the force when $\delta = 0$ mm and $\delta = 3$mm in Fig. 18.

According to equation (54), the base value of force is related to the remanence of the permanent magnet, thus if a larger holding force is needed, one can consider using rare-earth permanent magnets that have a larger remanence and better resistance to demagnetization.

VIII. CONCLUSION

This paper introduces the interpolating element-free Galerkin method to the application of magnetic field calculation. A modified weight function is proposed and its effectiveness is demonstrated by studying the magnetic field distribution of a novel permanent magnet bistable electromagnetic clutch. Compared with the traditional EFGM, the IEFGM is convenient to impose boundary conditions and only requires to employ fewer nodes to get accurate results, make the calculation efficiency higher. Based on the IEFGM, the magnetic field of the electromagnetic clutch is analyzed, an improved 2D analysis model is proposed. The improved 2D model solves the problem that the original 2D model cannot consider the magnetic flux leakage on the front and back region of the clutch. Then the force analysis of the clutch is carried out, and the holding force when the clutch in steady state is obtained. Finally, a clutch prototype experimental platform is built, and the experimental results verified the accuracy of the IEFGM in magnetic field analysis.

REFERENCES

[1] D. Daniel, *Application of the Element Free Galerkin Method to Elastic Rods*. Cambridge, MA, USA: Massachusetts Institute of Technology, 2000.

[2] Y. Y. Lu, T. Belytschko, and L. Gu, "A new implementation of the element free Galerkin method," *Comput. Methods Appl. Mech. Eng.*, vol. 113, nos. 3–4, pp. 397–414, Mar. 1994.

[3] T. Belytschko, Y. Krongauz, D. Organ, M. Fleming, and P. Krysl, "Meshless methods: An overview and recent developments," *Comput. Methods Appl. Mech. Eng.*, vol. 139, nos. 1–4, pp. 3–47, Dec. 1996.

[4] T. Belytschko, Y. Lu, and L. Gu, "Element-free Galerkin methods," *Int. J. Numer. Methods Engrg.*, vol. 37, no. 2, pp. 229–256, 1994.

[5] T. Belytschko, Y. Krongauz, M. Fleming, D. Organ, and W. K. Snm Liu, "Smoothing and accelerated computations in the element free Galerkin method," *J. Comput. Appl. Math.*, vol. 74, nos. 1–2, pp. 111–126, Nov. 1996.

[6] S. Liu, Q. Yang, H. Chen, G. Xu, and F. Liu, "Improvement of the element-free Galerkin method for electromagnetic field calculation," *IEEE Trans. Appiled Supercond.*, vol. 14, no. 2, pp. 1866–1869, Jun. 2004.

[7] H. Chen, Q. Yang, S. Liu, W. Yang, R. Yan, and W. Yan, "Element-free Galerkin modeling of giant magnetostrictive thin films," *IEEE Trans. Magn.*, vol. 41, no. 5, pp. 1512–1515, May 2005.

[8] E. H. R. Coppoli, R. C. Mesquita, and R. S. Silva, "Induction machines modeling with meshless methods," *IEEE Trans. Magn.*, vol. 48, no. 2, pp. 847–850, Feb. 2012.

[9] M. Arehpanahi and O. Vahedi, "Modified weight function with automatic node generation in element-free Galerkin method for magnetic field computation," *IET Sci., Meas. Technol.*, vol. 9, no. 8, pp. 1043–1049, Nov. 2015.

[10] Y. Fujita, S. Ikuno, T. Itoh, and H. Nakamura, "Modified improved interpolating moving least squares method for meshless approaches," *IEEE Trans. Magn.*, vol. 55, no. 6, pp. 1–4, Jun. 2019.

[11] Z. Zhang, P. Zhao, and K. M. Liew, "Improved element-free Galerkin method for two-dimensional potential problems," *Eng. Anal. Boundary Elements*, vol. 33, no. 4, pp. 547–554, Apr. 2009.

[12] Z. Zhang, S. Y. Hao, K. M. Liew, and Y. M. Cheng, "The improved element-free Galerkin method for two-dimensional elastodynamics problems," *Eng. Anal. Boundary Elements*, vol. 37, no. 12, pp. 1576–1584, Dec. 2013.

[13] H. Ren and Y. Cheng, "The interpolating element-free Galerkin (IEFG) method for two-dimensional potential problems," *Eng. Anal. Boundary Elements*, vol. 36, no. 5, pp. 873–880, May 2012.

[14] J. F. Wang, F. X. Sun, Y. M. Cheng, and A. X. Huang, "Error estimates for the interpolating moving least-squares method," *Appl. Math. Comput.*, vol. 245, pp. 321–342, Oct. 2014.

[15] D. Liu and Y. M. Cheng, "The interpolating element-free Galerkin (IEFG) method for three-dimensional potential problems," *Eng. Anal. Boundary Elements*, vol. 108, pp. 115–123, Nov. 2019.

[16] Y. M. Cheng, F. N. Bai, and M. J. Peng, "A novel interpolating element-free Galerkin (IEFG) method for two-dimensional elastoplasticity," *Appl. Math. Model.*, vol. 38, nos. 21–22, pp. 5187–5197, Nov. 2014.

[17] Q. Wu, F. B. Liu, and Y. M. Cheng, "The interpolating element-free Galerkin method for three-dimensional elastoplasticity problems," *Eng. Anal. Boundary Elements*, vol. 115, pp. 156–167, Jun. 2020.

[18] P. Xiong and C. L. Gu, "Starting assistance device for directly-driven electric vehicle with variable-idle speed control," *Teh. Vjesn.*, vol. 24, no. 1, pp. 209–216, Feb. 2017.

[19] P. Xiong and C. Gu, "An improved startup mode using clutch coupling for in-wheel electric vehicle drives," *Automatika*, vol. 58, no. 1, pp. 97–110, Aug. 2017.

[20] P. Xiong and C. L. Gu, "Experimental study of variable idle speed control for an in-wheel electric vehicle drive," *J. Engg. Res.*, vol. 7, no. 1, pp. 1–15, Mar. 2019.

[21] P. Xiong and C. L. Gu, "Research on torque compensation with optimal pedal throttle for direct-drive electric vehicle start-up," *Teh. Vjesn.*, vol. 24, no. 5, pp. 1391–1400, Oct. 2017.

FAN YANG received the B.S. degree in electrical engineering and automation from Hunan University, Changsha, China, in 2011. He is currently pursuing the Ph.D. degree with the School of Electrical and Electronic Engineering, Huazhong University of Science and Technology, Wuhan, China.

His research interests include electric vehicles, wheel motor design and control, electromagnetic devices, and magnetic field analysis.

CHENGLIN GU was born in Shangrao, Jiangxi, China, in 1954. He received the Ph.D. degree from the Huazhong University of Science and Technology, Wuhan, China, in 1989.

He has been a Visiting Professor with the University of Manchester Institute of Science and Technology (UMIST), U.K., since 1995. He is currently a Professor with the School of Electrical and Electronic Engineering, Huazhong University of Science and Technology. His research interests include new type of electric machines and drives, including synchronous reluctance motor and permanent magnet machines for electric vehicle applications.

Dr. Gu was a Founding Member with the International Society of Computational Magnetism (ICS). He was also a member of the Chinese Society of Electronics.